International Journal of Biological Macromolecules 311 (2025) 144007

Contents lists available at ScienceDirect

International Journal of Biological Macromolecules

journal homepage: www.elsevier.com/locate/ijbiomac

Role of lignin on microstructure, mechanical properties and flame retardancy of nanocellulose-based composite hydrogels

Aybüke Özkan [a], Ezgi Mıhlayanlar [a], Emine Ayşe Turhan [b], Ebru Sarıoğlu [a], Paul Berlu [a], Elif Kaynak [c,*], Erkan Senses [a,d,**]

[a] Department of Chemical and Biological Engineering, Koç University, Sariyer, Istanbul 34450, Türkiye
[b] Materials Science and Engineering, Koç University, Sariyer, Istanbul 34450, Türkiye
[c] Department of Civil, Environmental and Natural Resources Engineering, Luleå University of Technology, Luleå 97187, Sweden
[d] Koc University Boron and Advanced Materials Application and Research Center (KUBAM), Istanbul 34450, Türkiye

ARTICLE INFO

Keywords:
Cellulose nanocrystals (CNC)
Lignin
Borax
Flame-retardant
Hydrogel
Dynamic covalent bond
Fire prevention

ABSTRACT

Flame-retardant composite hydrogels provide significant advantages over conventional fire suppressants due to their high water retention, char-forming ability, and mechanical adaptability. However, the current formulations mostly rely on synthetic polymers or nanoparticles which restricts their large-scale application and reduces sustainability. In this work, we developed lignin-incorporated dynamically crosslinked cellulose nanocrystal (CNC) hydrogels and systematically investigated the interrelation between microstructure, rheological behavior, thermal properties, and flame-retardant performance. The incorporation of lignin at moderate concentrations enhanced hydrogen bonding, resulting in a denser and more homogeneous hydrogel network with reduced mesh size. The resulting elastic network enhanced water retention during burning, promoting flame retardancy via substrate cooling and fuel dilution effects. Additionally, lignin facilitated the formation of a compact glassy char layer, effectively serving as a heat and oxygen barrier. Thermal decomposition of dried CNC films resulted in 8.6 % residue at 700 °C, whereas CNC-lignin-borax composites exhibited a significant increase in char yield, reaching 70.5 %. The optimal lignin composition extended burn-through time of wood to 12 min—71 % and 33 % longer than uncoated and neat CNC samples. Our findings highlight the potential of CNC-borax-lignin hydrogels as biorenewable environmentally friendly coatings with superior flame-retardant properties, offering a sustainable approach to fire prevention in wood-based materials.

1. Introduction

Fires are some of the most devastating disasters, whether natural or caused by human activity, posing serious risks to lives, ecosystems, and infrastructure worldwide [1]. In forests, farmlands, and cities, they spread rapidly due to the availability of flammable materials, oxygen, and heat, leaving behind widespread environmental destruction and heavy economic losses [2]. Conventional fire suppression methods, such as water treatments, chemical powders, and halogenated flame retardants, have been widely used, but they come with limitations such as insufficient cooling efficiency, environmental toxicity, restricted long-term performance, and limited reusability [3,4]. These limitations have driven the search for sustainable and eco-friendly flame-retardant materials.

Hydrogels have emerged as practical materials for fire prevention because of their significant water retention ability inherent to their network structure [5], self-repairing capabilities originating from reversible bonds [6], and outstanding barrier properties [7,8]. When subjected to fire, the water in the hydrogel structure transforms into vapor, cooling down the substrate and lowering oxygen levels in the surrounding area [9,10]. Hydrogels bond effectively to surfaces, forming a barrier for thermal and mass transfer which prevents the spread of flames [11–13]. Most hydrogel systems reported rely on synthetic polymers or inorganic nanoparticles, raising concerns regarding their environmental persistence, contribution to microplastic pollution and challenges in sustainable production [7,14,15]. Moreover, many hydrogels function only when hydrated, requiring frequent rehydration to maintain fire resistance properties [16,17]. This limitation restricts

* Correspondence to: E. Kaynak, Department of Civil, Environmental and Natural Resources Engineering, Luleå University of Technology, Luleå 97187, Sweden
** Correspondence to: E. Senses, Department of Chemical and Biological Engineering, Koç University, Sariyer, Istanbul 34450, Türkiye.
E-mail addresses: elif.kaynak@associated.ltu.se (E. Kaynak), esenses@ku.edu.tr (E. Senses).

https://doi.org/10.1016/j.ijbiomac.2025.144007
Received 28 February 2025; Received in revised form 23 April 2025; Accepted 5 May 2025
Available online 6 May 2025
0141-8130/© 2025 The Authors. Published by Elsevier B.V. This is an open access article under the CC BY license (http://creativecommons.org/licenses/by/4.0/).

their prolonged or extensive applications, particularly in high-temperature environments where water rapidly evaporates, demanding the development of new materials that can provide extended protection through synergistic and combined flame retardant mechanisms [18–20]. These challenges have increased the importance of environmentally friendly, biodegradable and sustainable alternatives in the development of fire-resistant materials. In particular, the limited functionality of existing hydrogel systems that are only effective in the presence of water and the environmental impact of their synthetic ingredients highlight the potential of using nature-derived components. Among these materials, ligninstands out as a promising candidate in the design of sustainable fire-retardant hydrogel systems [21,22].

Lignin, the most abundant natural biopolymer after cellulose, plays a crucial role in plant cell walls by providing structural support and protection against environmental stresses. It is a by-product of the cellulose pulping process and has traditionally been considered as waste. However, its chemical composition, rich in aromatic rings and functional groups, allows it to generate char efficiently during thermal degradation [23,24]. This char formation makes a protective barrier that limits the flow of heat and oxygen, thus significantly enhancing flame retardancy [25–29]. Moreover, it serves as a char-forming agent in intumescent flame-retardant systems for polymeric materials, exhibiting a synergistic effect when combined with other flame-retardant substances, thereby making it an essential component in the development of bio-based, environmentally friendly fire-resistant systems. [18,30,31]. Lignin structure was shown to reduce the release of flammable gases during combustion by promoting char formation [19,32]. When lignin is added to polymer matrices such as polylactic acid (PLA) and polyurethane (PU), the thermal stability is increased and lower heat release was found during combustion [33]. In addition, coatings containing sodium lignin sulfonate (SLS) showed a successful flame-retardant effect on cotton fabrics and increased the thermal stability of these fabrics [34,35]. Intumescent systems using lignin and phosphinates were shown to slow down combustion and promote carbonization in engineering plastics such as polyamide [36]. However, these synergistic effects have been mostly explored in solid-state systems, while their application in hydrogel matrices remains relatively underexplored.

Our previous study have investigated borax cross-linked CNC hydrogels [37] this study aims to develop a functionally improved hydrogel system where lignin is included as a third and synergistic component. Incorporating lignin into CNC-borax hydrogels is anticipated to create a synergistic effect, combining lignin's char-forming capabilities with borax's cooling and barrier properties [38–40]. In addition to this, it is expected that lignin addition introduces new molecular interactions that affect the microstructure, mechanical behavior, and water retention capacity of the hydrogel. This interaction has the potential to produce hydrogels that provide superior thermal stability, higher flame suppression efficiency, and better fire safety. By exploring the effect of lignin incorporation on microstructure and fire resistance, we aim to develop high-performance flame-retardant material for protective coatings. This approach holds strong potential for the development of next-generation multifunctional hydrogels with superior flame resistance, mechanical strength, and environmental compatibility, aligning by valorizing biomass resources and advancing bio-based material design.

2. Materials and methods

2.1. Materials

Nanocrystalline cellulose (CNC) derived from wood, supplied by CelluForce (Montreal, Canada), was utilized in its spray-dried form, exhibiting an approximate crystalline density of 0.88 and a hydrodynamic diameter of approximately 70 nm. The molecular weight of the CNC ranged between 14,700 and 27,850 g/mol, and its zeta potential was measured at −37 mV, according to the supplier's specifications. Borax ($Na_2B_4O_7{\cdot}10H_2O$), with a molar mass of 381.37 g/mol and a purity of 99.5 %, was procured from Sentez Laboratory Chemicals and Devices (Istanbul, Turkey). Lignin derived from kraft softwood was supplied by UPM Biochemicals (Helsinki, Finland). The molecular weight of the lignin ranged between 5000 and 6000 g/mol. All materials were used as received, without further purification.

2.2. Preparation of CNC-lignin-borax hydrogels

Aqueous solutions of lignin were prepared by gradually dispersing the lignin in deionized water. To facilitate this, lignin was slowly added to water continuously stirred with a magnetic stirrer to generate a vortex. Subsequently, CNC powder was incorporated into the lignin solution, with Lignin/CNC weight ratios set at 0, 0.5, and 1. The solution was stirred overnight on a magnetic stirrer to ensure homogeneity. To induce gelation, the borax powder was gradually added to 10 ml of the CNC-lignin solution under stirring. The amount of borax powder was adjusted based on the CNC content in the 10 ml solution, keeping the Borax/CNC weight ratio at 2 as described in our previous study [37]. All the samples were sealed to prevent evaporation and stored at room temperature for 24 h to allow the system to reach equilibrium before characterization (see Supporting Information for the stability analysis). The samples were labeled as “X CNC-Y Lignin-Z Borax” (or in the short form: X CNC-Y L-Z B" where X indicates the percent mass of the CNC in water used to prepare the hydrogel sample, Y signifies the Lignin/CNC weight ratio and Z represents the Borax/CNC weight ratio in each sample.

2.3. Fourier-transform infrared spectroscopy

Fourier-transform infrared (FTIR) analysis was conducted using a Thermo Fisher Scientific (USA) Nicolet iS10 FTIR spectrometer equipped with a DTGS KBr detector. Samples in gel phase or dried form (the neat component) were scanned over a spectral range of 400 to 4000 cm^{-1}, with 64 scans collected per measurement. The data were reported in terms of transmittance (%).

2.4. Polarized optical microscopy

Polarized optical microscopy images of gel samples were taken by Bresser MicroCam SP5. Polarizing Light Microscope equipped with polarized film. Images were acquired using MicroCamLabII Software.

2.5. Scanning electron microscopy

The samples were freeze-dried under vacuum for 48 h until completely dried. Scanning Electron Microscopy (SEM) was conducted on the cross-sections of the freeze-fractured samples with a Zeiss Ultra Plus Field Emission Scanning Electron Microscope, operating at voltages of 3 kV.

2.6. X-ray photoelectron spectroscopy

The chemical composition and elemental states of the hydrogels were analyzed using X-ray photoelectron spectroscopy (XPS). Measurements were conducted with a Thermo K-Alpha X-ray Photoelectron Spectrometer (Thermo Fisher Scientific, USA) under ultra-high vacuum conditions. The survey and high-resolution spectra were recorded to determine the elemental composition and the oxidation states of carbon, oxygen, and other relevant elements in the hydrogels. The binding energy scale was calibrated using the C 1 s peak at 284.8 eV. Data analysis and peak fitting were performed using Avantage software (version 6.6.0, Thermo Fisher Scientific).

2.7. Rheology

Rheological measurements were conducted using an Anton Paar MCR-302 rheometer with a 25 mm parallel plate and solvent trap, maintaining a 1 mm gap. The temperature was held constant at 25 °C using a Peltier system with a temperature control hood to minimize heat loss and prevent sample evaporation. Samples were freshly prepared and tested following a 24-h rest period. Amplitude sweep tests were performed to establish the limits of the linear viscoelastic region (LVE), with the linearity limit set at a 10 % deviation from the storage modulus (G′) to ensure the sample structure remained undestroyed. Frequency sweep tests provided viscoelastic property data as a function of time-scale, using previously determined linearity limits from the amplitude sweep as the constant shear strain amplitude to maintain the LVE region. Angular frequency varied from 0.1 to 10 rad/s for each sample, and responses of the storage modulus (G′), loss modulus (G″), and complex viscosity (η) were recorded.

Large amplitude oscillatory shear (LAOS) tests were then conducted to examine material response in the non-linear viscoelastic region, where large strains altered the material's inherent structure. In contrast to frequency sweeps, where small strains preserved the LVE region, LAOS involved strain amplitudes from 0.01 to 1000 % with a constant angular frequency of 10 rad/s. Angular frequency and temperature remained constant ($\omega = 10$ rad/s, $T = 25$ °C), with corresponding G′ and G″ values recorded.

To evaluate the long-term stability of CNC-L-B hydrogels, rheological measurements were conducted at different time points. These experiments were designed to clarify whether the systems remain stable beyond the initial 24-h resting period stated in the manuscript. Viscosity tests were performed using an MCR-302 rheometer (Anton Paar, Austria) equipped with a 25 mm diameter parallel plate geometry. To prevent water evaporation during the measurement process, a solvent trap was used to maintain a saturated environment around the sample. All measurements were conducted at room temperature over a shear rate range of 0.01 to 100 s^{-1}, under steady-state conditions. Two different sets of formulations were investigated. The first group consisted of sol-state samples without Borax: 5CNC-0 L-0B, 5CNC-0.5 L-0B, and 5CNC-1 L-0B. Their viscosities were measured immediately after preparation (Day 0), then after 24 h (Day 1), and 48 h (Day 2). The second group included hydrogel formulations with Borax as a crosslinker: 5CNC-0 L-2B, 5CNC-0.5 L-2B, and 5CNC-1 L-2B. These samples were tested at 24 h (Day 1), 48 h (Day 2), and 72 h (Day 3) after preparation.

2.8. Adhesion test

Adhesion of the samples at sol and gel-states was assessed using wood substrates. Rectangular wooden blocks with a length of 10 cm were used as the adhesion substrate. A 1.5 cm section from the bottom end of each stick was marked to define the contact area. A total of 0.8 g of each hydrogel or sol-state formulation was applied to this marked region. Six different formulations were tested, each containing different amounts of lignin and borax. After application, the samples were suspended vertically to enable visual comparison of their dripping behavior and adhesion performance.

2.9. Thermogravimetric analysis

Thermal analysis of the gel samples was performed using a simultaneous TGA/DSC instrument (Q500, TA Instruments, USA), heating the samples up to 800 °C at a constant of 10 °C/min under 100 ml/min nitrogen flow. Approximately 10 mg of each sample was placed into an alumina sample cup for the analysis.

2.10. Thermal profile analysis

The thermal response of hydrogel samples was analyzed by monitoring temperature profiles on a controlled hot plate up to 90 °C. The hot plate utilized for this study was equipped with integrated temperature control with an accuracy of ±0.2 °C. Each hydrogel sample was carefully positioned at the center of a glass slide, with a mark at the center to ensure consistent alignment for the measurements. A silicone mold with a predefined disc-shaped hole (6.99 mm diameter, 2.40 mm thickness) was used to ensure uniform sample dimensions, allowing for a constant mass distribution across each sample. A ceramic plate was placed on the hot plate (ISOLAB, Magnetic Stirrer with Hot-Plate) to avoid short-ranged temperature fluctuations of the substrate. The glass slide with the sample was placed on the ceramic surface, and its position was centered and marked with a pen for alignment. A thermal camera (HIKMICRO, Pocket Thermography Camera) was positioned 25 cm above the glass slide. The camera was aligned to the glass slide to focus on the sample's center, capturing temperature data at 15-s intervals for each sample. The blank sample consisted only of the glass slide; the capture time was set to 5-s intervals as the temperature reached 90 °C more quickly. Distilled water was also tested for comparison. Once the hot plate temperature is stabilized, the sample was placed on the designated mark, and thermal data was recorded for 20 min. Temperature readings from the thermal camera are consistently collected from the center of each sample. The data recorded provided a basis for plotting the temperature (°C) as a function of time (minutes), allowing for an evaluation of the cooling properties of the hydrogels.

2.11. Drying test

A drying test was designed to evaluate the water retention performance of the hydrogels. Time-dependent weight changes were recorded using a precision balance (Radwag AS 220.R2 with readability of 0.1 mg and standard repeatability 0.08 mg). Hydrogel samples of 12 mg were tested under room conditions at 23 ± 0.2 °C and 36 ± 1 % relative humidity, with weight recorded at 1-min intervals. Weight change versus time plots were generated, and water loss rates during the first 10 min were calculated.

2.12. Flammability tests

The flammability of hydrogels and hydrogel-coated substrates was assessed using various set-ups specifically designed to measure different flame retardancy properties.

The charring ability of gels was studied by blowtorch (Orcamp, Türkiye) flame impingement. The gel sample was transferred to the flat end of a spoon using a silicone mold (hole diameter = 10 mm, height = 3 mm) to give a consistent disk-shaped sample. The spoon containing the sample was secured above and parallel to the horizontal plane from the other end. The torch was positioned at a 45-degree angle to ensure a 5 cm center-to-center distance between the barrel's tip and the spoon's surface. The flow rate of the gas (70 % butane, 30 % propane) was fixed using the knob. The flame was applied for 30 s from the top at a 45-degree angle. The digital images of the samples before and after flame impingement were taken using a lab-made optical goniometer attached to a USB digital microscope camera (Microcase).

A custom-made burn-through set-up was used to quantify the fire resistance provided by the gel coating. A blowtorch (Orcamp, Turkey) fueled by a propane-butane mixture, which can develop a maximum flame temperature of 1300 °C according to the manufacturer's specifications, was positioned upward at a 45-degree angle. Pinewood blocks (165 mm × 165 mm × 16 mm) were obtained from a local carpenter and used as substrates. The specimen was secured at a 45-degree angle with clamps at 1 cm from both sides so that the torch flame was perpendicular to and passed through the center of the specimen. A circular area with a 40 mm radius was coated with 1 mm thickness 30 g of gel at the center of the block's front surface, while a 5 mm radius circle was marked at the center of the block's rear surface. During testing, the torch flame was applied continuously. The burn-through time was defined as the

duration from the ignition of the torch until the char fills the marked circle on the rear surface of the block.

The vertical flame progression and fire-prevention performance of the gels were evaluated using thin, flat bamboo bars (2 cm × 24 cm × 2 mm) as substrates. The specimen was placed vertically and was marked at intervals starting from 2.5 cm, with additional markings every 2.5 cm up to the halfway point. The top half of the bar was coated with 1–2 g of gel on both surfaces. The bottom of the bar was exposed to a flame (6 cm heigh with 45 °C angle) generated by blowtorch (Orcamp, Türkiye) for 10 s. The flame progression from the ignited bottom section to the gel-coated area was monitored until the flames were extinguished and the combustion ceased. The test was repeated six times for 1-g gel coated wet sample and three times for 2-g gel coated wet sample to verify the flame progression behavior. Then, the 2-g gel-coated sticks were dried in the oven for 1 h at 60 °C to evaluate the char-forming efficiency of the dry film. After drying, the wooden bars were exposed to a flame application for 10 s, and their burning behavior was observed and reported.

A custom-made 45-degree flammability test set-up (67) was used to assess the ease of extinction in gel-coated samples. 45-degree angle was chosen such that relatively slow flame progression can be observed, and the excessive heating of the upper uncoated wood portion can be eliminated. Square bamboo sticks (3 mm × 3 mm), 18 cm long, were marked starting 10 cm from the bottom of the specimens (lower reference mark), with a 3 cm portion along the length marked at 0.5 cm intervals. An alcohol lamp containing ethanol (99.6 %) was used to ensure a consistent 3 cm flame height during the test. The specimen was clamped to the horizontal plane from the upper 4 cm at a 45-degree angle. The burner was positioned on the horizontal plane with the top of the burner barrel 3 cm below the center of the bottom edge of the specimen. The flame was applied for 10 s. An up-down method was used to determine the effect of gel coat length on extinguishing flames. In the up-and-down procedure, a particular portion above the lower reference mark was coated with the gel. In this test, the gel mass applied changed proportionally to the coating length, i.e. 25 mg gel was applied on the 5.0 mm portion of the stick. When the coating length was doubled, the gel mass also doubled to keep the coating density unchanged. If the flames passed beyond the gel-coated portion, the coating length was increased; if the flames extinguished on the gel-coated portion, the coating length was decreased. This was repeated until the coating length between two consecutive responses (i.e., extinguished, sustained flaming) differed by 2.5 mm. Then, two more specimens were tested with the gel coating at the minimum length found to be sufficient to extinguish the flames. The minimum coating length was recorded if the flames were extinguished in both tests.

All the substrates (bamboo and pine wood) were conditioned at 50 % RH and 23 °C for at least 48 h before testing for consistency.

3. Results and discussion

3.1. The microstructure and interactions in the CNC-lignin-borax hydrogels

We first investigated the interaction between the components and the resulting microstructure. In a previous study on 3 % and 5 % CNC hydrogels, 5 % CNC gels were significantly effective for flame retardancy, thus we focus primarily on 5 % CNC concentrations in this work [37]. Borax/CNC ratio was also important, especially for the mechanical and thermal behavior of the hydrogels. Low borax concentrations were not preferred because they did not show sufficient flame-retardant effect, while high borax concentrations led to phase separation and loss of homogeneity in the hydrogel structure. Thus, the concentration of borax/CNC weight ratio was fixed at 2 to improve the fire extinction performance while still forming a consistent CNC hydrogel network through dynamic boron-ester bonds. To elucidate the effect of lignin, lignin/CNC weight ratio of 0.5 and 1 were selected to ensure a homogeneous distribution in the hydrogel structure while optimizing the lignin concentration to reveal its combined or synergistic effects with CNC and borax on fire prevention.

Fig. 1 shows a bonding mechanism involving CNC, lignin, and borate ions to form a hydrogel. In the CNC-lignin-borax hydrogel system, the dissolution of borax in water yields boric acid ($B(OH)_3$) and tetrahydroxyborate ions ($B(OH)_4^-$). These ions are reactive and interact with the hydroxyl groups of cellulose nanocrystals (CNCs) to form boronate ester bonds, linking the CNCs to form a three-dimensional network, and resulting in the transition of CNC dispersion from a liquid state to a gel-like form (see the inverted vial images below). The borax-induced crosslinking enhances the structural integrity of the hydrogel, creating a network that holds its shape, providing stability and rigidity to the hydrogel. Lignin, with its hydroxyl groups, contributes to the network formation by forming hydrogen bonds.

FTIR spectra of the freeze-dried samples were shown in Fig. 2A and B and gel-state versions were shown in Fig. S1. FTIR spectroscopy revealed the key interactions within the hydrogels, particularly the formation of boronate ester linkages. The individual components of the hydrogels—CNC, lignin, and borax were analyzed separately (Figs. S1A, S1B, and S1C) with their main peaks detailed in Table S1. In the borax-free samples (5CNC-0 L-0B, 5CNC-0.5 L-0B, and 5CNC-1 L-0B), the addition of lignin to the 5 % CNC solution resulted in new peaks at 1720 cm^{-1} (C═O stretching) and 1596 cm^{-1} and 1507 cm^{-1} (aromatic ring vibrations), confirming lignin incorporation, as shown in Fig. 2A. The intensity of the 1317 cm^{-1} peak (CH_2 in amorphous cellulose) decreased, while the broad 3300 cm^{-1} OH peak diminished, indicating hydrogen bonding between lignin and cellulose and a reduction in free hydroxyl groups.

Upon borax addition, the presence of boronate ester linkages was further confirmed by characteristic peaks at 1335 cm^{-1}, 1430 cm^{-1}, and 824 cm^{-1} (BO_3 group vibration), consistent with previous studies [37,41–46]. Incorporating lignin into the system enhances crosslinking through hydrogen bonds with CNCs and borax [29]. Thus, borax-containing samples exhibited a carbonyl shift from 1720 cm^{-1} to 1658 cm^{-1}, indicating borax-lignin interactions, while the decreased both 3330 cm^{-1} OH peak and the 824 cm^{-1} peak confirmed hydroxyl group reduction. The higher lignin content in the 5CNC-1 L-2B samples may lead to increased competition for borate groups, leading to preferential interaction with lignin rather than cellulose. This competition could account for the observed decrease in the intensity of the 1335 cm^{-1} peak and has important conclusions in terms of microstructure and rheological behavior as explained in the next section.

To better understand the chemical composition and elemental states of the hydrogels, XPS analysis was conducted. Fig. S2A shows the profile for neat 5 % CNC (5CNC-0 L-0B), with the highest intensity at C1 (284.5 eV) and C2 (286.16 eV), consistent with cellulose nanocrystals. Minor peaks (C3, C4, C5) remained relatively low [47]. These peaks correspond to: C1 (284.31–284.94 eV) – C–C/C–H bonds; C2 (286.11–286.23 eV) – C—O in cellulose; C3 (287.72–287.81 eV) – C═O groups; and C4 (288.28–289.46 eV) –carboxylates and esters from oxidation or residual polysaccharides [48,49]. In borax-free samples, the decrease in C—C (C1) intensity and increase in oxygen content in lignin-containing samples (5CNC-0.5 L-0B, 5CNC-1 L-0B) result from lignin's hydroxyl, methoxy, and carbonyl groups. Lignin also altered carbon bonding, increasing C2 (C—O) and C3 (C=O) peak intensities as seen in Table S2. The oxygen content rose from 19.86 % in 5CNC-0 L-0B to 37.7 % in 5CNC-0.5 L-0B and 40.84 % in 5CNC-1 L-0B, respectively, confirming lignin's role in surface oxygenation [50]. Furthermore, in borax-free samples, a single O1s peak (O2) at ~532.53–532.6 eV (Fig. 2C) indicated a homogeneous oxygen environment, primarily from hydroxyl (-OH) and ether (-C-O-C-) groups in CNC and lignin. The addition of borax increased the number of ether bonding, with oxygen in the boroester structure bonding to carbon, strengthening the C2 linkage. As a result, the C2 content was increased from 20.84 % in 5CNC-0 L-0B to 30 % in 5CNC-0 L-2B. Moreover, there was a notable decrease in non-oxygenated carbon (C1) in the samples 5CNC-0 L-2B compared to

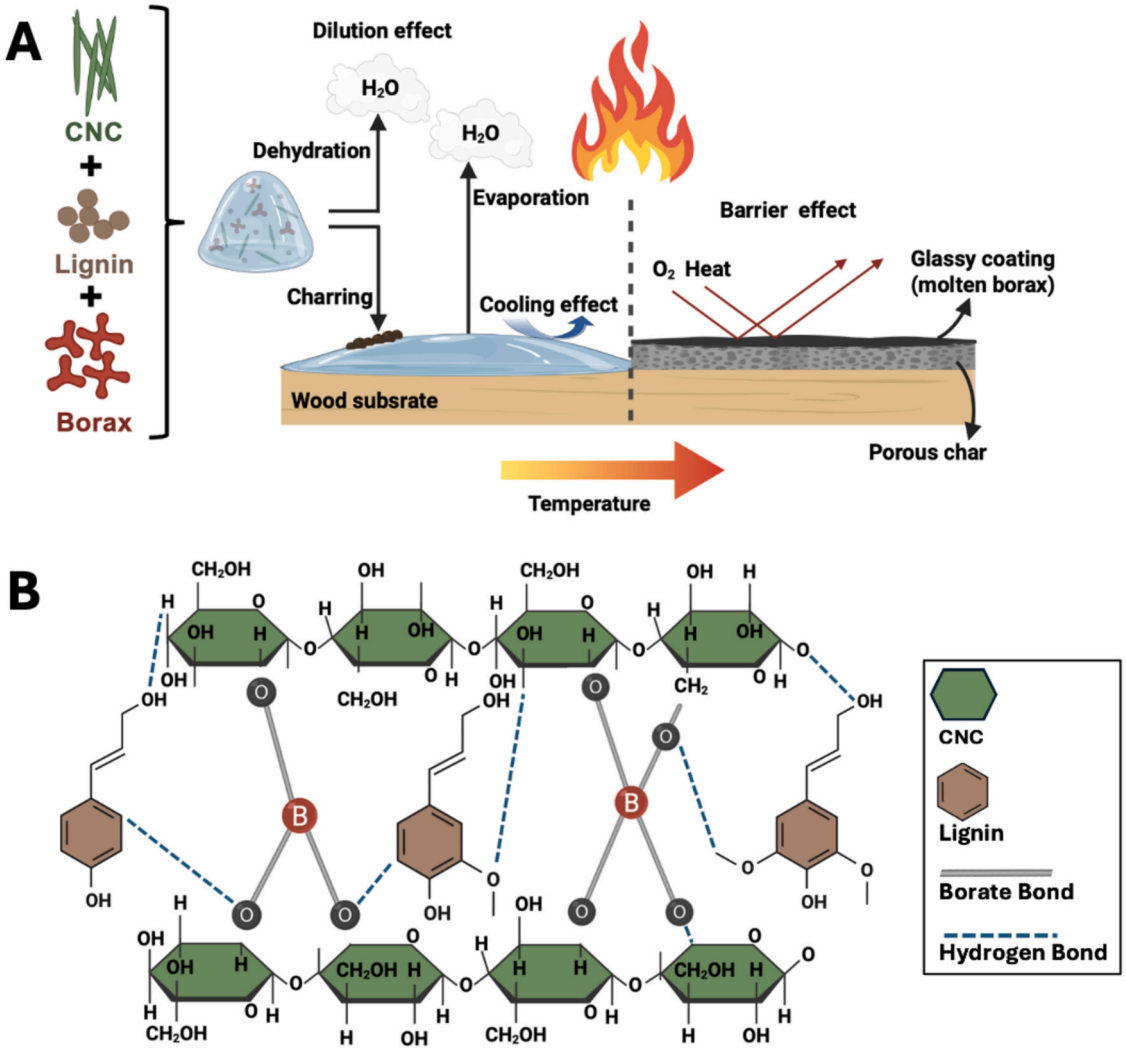


Fig. 1. (A) Schematics of the components of flame-retardant hydrogel and proposed mechanisms for fire prevention, and (B) the bonding interactions between CNC, lignin and borax.

5CNC-0 L-0B, and variations in oxygenated carbon groups (C2 and C3), reflecting its role in crosslinking and structural changes. Furthermore, the oxygen environment was changed significantly, as evidenced by the splitting of the O1s peak into three distinct components (Fig. 2D–F): O1 (531.3–531.5 eV) for B—O bonds, O2 (532.5–532.67 eV) for –OH and –C–O–C– groups, and O3 (535.66–535.71 eV) for adsorbed water. The presence of B–O–B bonds at 191–192 eV range confirmed boroester formation between borax and cellulose [49,51]. In 5CNC-0 L-2B, boron content was 8.73 %, increasing to 9.09 % in 5CNC-0.5 L-2B, reflected in the O1 peak rising from 11.02 % to 12.46 %. In contrast, 5CNC-1 L-2B sample showed a decrease in the O1 peak, suggesting fewer B—O bonds—which can be attributed to structural disruptions and reduced boron-cellulose interactions caused by lignin agglomeration, as also indicated by the FTIR results.

In summary, FTIR results confirmed successful incorporation of lignin and borax into the CNC hydrogel, and formation of hydrogen bonding, and dynamic boronate ester linkages. Complementary XPS analysis supported these findings by revealing changes in carbon and oxygen bonding environments, increased surface oxygenation due to lignin, and the formation of B—O and B–O–C bonds in borax-containing samples. Together, these analyses verify the formation of a physically crosslinked CNC-borax-lignin network.

We then examined the microstructures of the samples (in freeze-dried forms) using Scanning Electron Microscopy (SEM) and Polarized Optical Microscopy (POM). Fig. 3A and B show images of hydrogels with and without borax, each sample containing varying lignin contents. The POM images in the top row of Fig. 3A illustrate differences in crystallinity across the samples that contain no borax (i.e. the sol states). The lignin-free sample (5CNC-0 L-0B) displays consistent alternating birefringence and dark layers typical of the homogenous biphasic state of concentrated CNC solutions [52], suggesting well-dispersed CNCs with only a few small CNC clusters identified as bright crystalline spots [53]. When lignin is introduced, the birefringence gradually disappears while more significant fractions of micron-sized CNC clusters and some spherical-shaped lignin aggregates (seen as dark brown spots) appear. The brown color of the matrix increases with lignin content due to the increased fraction of soluble lignin found together with CNC in water. At the highest lignin concentration (5CNC-1 L-0B), optical clarity is reduced, and more lignin precipitates are found, indicating that higher lignin levels contribute to a more disordered structure. The presence of the lignin clusters in the CNC network has a strong and unprecedented influence on rheology and flame retardancy as described later. The SEM images of the freeze-dried samples in Fig. 3A (bottom row) show the mesoscale morphological changes due to lignin addition in borax-free samples. Without lignin, the CNC hydrogel (5CNC-0 L-0B) displays a compact and layered structure with minimal porosity. The addition of lignin (5CNC-0.5 L-0B) helps to form porous structures due to the destabilization of CNC dispersion and clustering which may act as

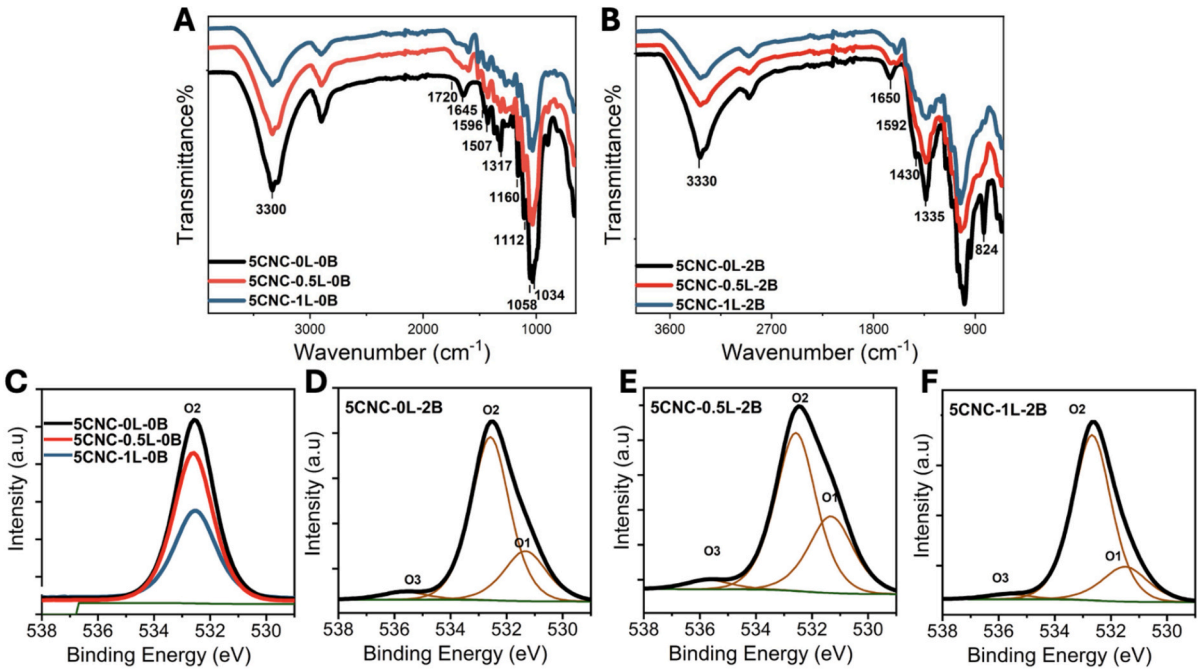


Fig. 2. Fourier-transform infrared (FTIR) spectra for: (A) 5CNC-0 L-0B, 5CNC-0.5 L-0B, and 5CNC-1 L-0B; (B) These groups after adding borax, resulting in 5CNC-0 L-2B, 5CNC-0.5 L-2B, and 5CNC-1 L-2B samples. X-Ray Photoelectron Spectroscopy (XPS) spectra for: %O component of (C) samples without borax, (D) 5CNC-0 L-2B, (E) 5CNC-0.5 L-2B, (F) 5CNC-1 L-2B.

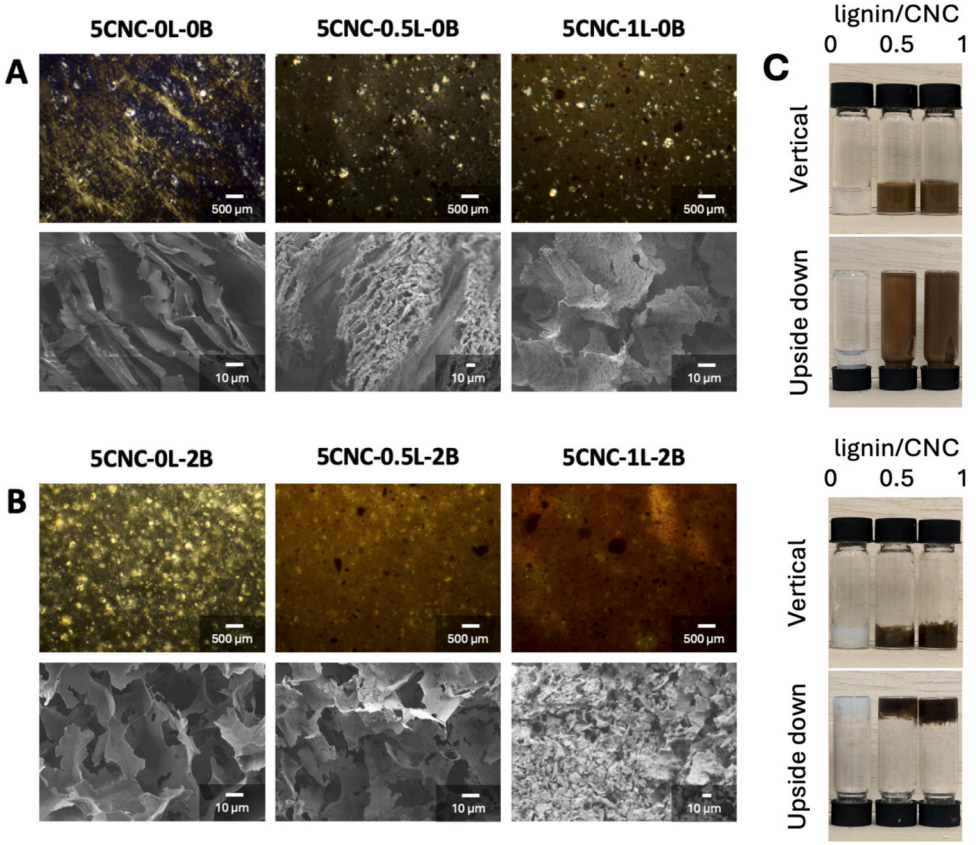


Fig. 3. Polarized optical microscopy and SEM images of samples: (A) 5CNC-0 L-0B, 5CNC-0.5 L-0B, and 5CNC-1 L-0B; (B) 5CNC-0 L-2B, 5CNC-0.5 L-2B, and 5CNC-1 L-2B. (C) Representative images of the borax-free sol samples and borax-containing gel samples in vertical and inverted positions.

physical crosslinks. Nevertheless, these compact and porous structures remain isolated and not percolated through the samples, thus the composite remains in sol-state. With the increase in the amount of lignin (5CNC-1 L-0B), very large and open pores are formed due to increased bonding sites. Still the samples in the absence of borax crosslinker remain in sol state.

The POM images in Fig. 3B show a noticeable change in microstructure with borax incorporation. Upon the addition of borax, the lignin-free CNC suspensions turn into gels almost immediately. Fig. 3C shows the sol-gel transition of the CNC-lignin composite suspensions. The gel network is formed via the dynamic boron-ester bonds. In the absence of lignin, the excess, undissolved borax crystals are dispersed relatively uniformly throughout the gel. These borax crystals can reinforce the gels and form a protective glassy layer upon melting and solidification in the event of a fire [37]. As lignin content increases, the amount and size of clusters increased while the transparency of the gels significantly decreased compared to the borax-free sol samples in Fig. 3A. There was no indication of macroscopic phase separation of any component in the gels. The SEM images in Fig. 3B show the gel network structure of borax containing samples. In the lignin-free case, adding borax creates a relatively uniform porous structure as opposed to its borax-free form, confirming the homogenous gel formation with boron-ester bonds. In the sample with moderate lignin amount (5CNC-0.5 L-2B), the hydrogel displays smaller-sized pores and denser (but still quite uniform) arrangement with interconnected CNC sheets, suggesting a tighter bonding due to additional boron-ester bonds between the -OH groups of the lignin and the borates. On the other hand, with higher lignin content (5CNC-1 L-2B), the porous structure breaks down, leading to a heterogeneous state consisting of densely packed zones interspersed with porous regions. Unlike this, the borax-free sol state of the same composition (5CNC-1 L-0B) displayed a uniform porous structure. Thus, in the case of large fractions of lignin, the addition of borax, while inducing gelation, may lead to lignin/CNC phase separation which may have important implications in the viscoelastic behavior of the composite hydrogels and fire prevention performance.

3.2. Rheological behavior of CNC-lignin-borax hydrogels

The interaction between CNCs, lignin, and borax significantly affects the stability, elasticity, and microstructure of the composites. These properties are key for optimizing the viscoelastic properties of the gels, which affects their water-holding and release capacity, injectability and sprayability, surface adhesion and spreading, all of which ultimately govern their fire prevention performance. Fig. 4 compares samples with and without borax using oscillatory rheology with dynamic frequency sweep tests. It illustrates how the storage modulus (G', elastic behavior) and the loss modulus (G“, quantifying viscous liquid behavior) change with frequency for borax-free CNC-lignin composite suspensions with varying lignin levels. The neat CNC suspension displays a typical viscoelastic behavior with G" > G' at the low frequencies and G' dominates the high frequency region. More importantly, the moduli are strongly frequency-dependent and the cross-over where the liquid-to-solid transition occurs is observed at about 1 rad/s, consistent with the previous findings. [54,55]. The moduli range between 1 Pa and 10 Pa, indicating the soft and weak nature of these viscoelastic liquids. Lignin addition to CNC suspensions substantially changes the viscoelastic behavior. It is observed that both G' and G“ shift to higher values as lignin concentration increases. More importantly, lignin gradually turns the viscoelastic CNC suspensions into soft solids as G' exceeds G" at all frequencies and the dependence of moduli on frequency becomes weaker. The storage moduli of the lignin-containing samples are about 20 and 60 times higher (but remain below 100 Pa) compared to the neat CNC at the low-frequency regime. The reinforcement effect of lignin is primarily due to additional crosslinking provided by the amorphous structure of lignin via hydrogen bonds and van der Waals forces [56]. The changes in network structure are also evidenced by the sample

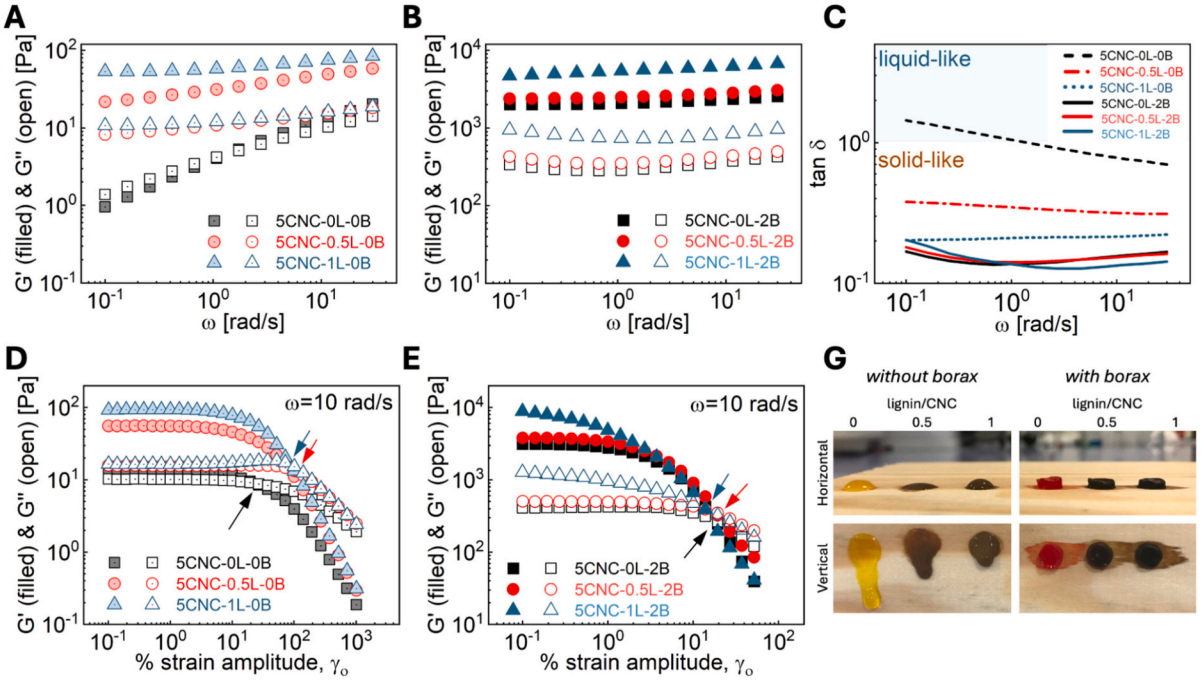


Fig. 4. Filled (G′) and Open (G″) modulus as a function of angular frequency for: (A) CNC-L-B gels prepared from 5 wt% CNC with increasing lignin concentrations; (B) CNC-L-B gels prepared from 5 wt% CNC solutions and constant borax/CNC = 2 weight ratios with increasing lignin concentrations. (C) Loss factor as a function of angular frequency. Filled (G′) and Open (G″) modulus as a function of amplitude sweep responses for: (D) CNC-L-B gels prepared from 5 wt% CNC with increasing lignin concentrations; (E) CNC-L-B gels prepared from 5 wt% CNC solutions and constant borax/CNC = 2 weight ratios with increasing lignin concentrations. (G) Visual representation of spreading application of CNC-B-L samples prepared from 5 wt% CNC solutions and constant borax/CNC = 0 and 2 weight ratios with increasing lignin concentrations on wood surfaces on the horizontal level and their behavior when placed upright on a vertical position. A trace amount of commercial food colorant was used to aid visual assessment.

images and POM micrographs presented in Fig. 3. In addition, the presence of large, micron-sized lignin clusters may strengthen the gels as they can behave as fillers, however, their fraction is relatively low, thus, it plays a minor role for these borax-free samples.

Borax addition yields boronate ester bonds between CNC and borax, resulting in dynamically crosslinked CNC networks, as explained in the morphology and interaction section. The CNC gel cross-linked via boronate ester bonds (5CNC-0 L-2B) exhibits an elastic modulus of approximately 2.5 kPa that is over three orders of magnitude greater compared to the borax-free samples (5CNC-0 L-0B). The resulting material is a gel characterized by a frequency-independent elastic modulus that exceeds the loss modulus at all frequencies shown in Fig. 4B. With the addition of lignin, the modulus slightly increases in 5CNC-0.5 L-2B, as the addition of lignin does not disrupt the network structure but the pore size dimmish, leading to stiffening (Fig. 4B). On the other hand, further increasing the lignin content shifted the modulus of the CNC-borax hydrogel (5CNC-1 L-2B) by approximately four times due to lignin agglomerations observed in the gel (Fig. 4B), which acts as reinforcing fillers for the gel network. We also calculated the loss factor ($\tan\delta = G''/G'$) as a function of angular frequency to better understand the viscoelastic characteristics of the samples. As presented in Fig. 4C, $\tan\delta < 1$ indicates a solid-like structure, while higher values shift toward liquid-like behavior. In samples without borax, tan δ increases as frequency decreases, especially in those with less lignin, indicating a tendency toward more liquid-like behavior at lower frequencies. However, the 5CNC-1 L-0B sample maintains a solid-like structure across all frequencies, suggesting that higher lignin content contributes to network stability. Tan δ values stay lower throughout the frequency range in samples containing borax, suggesting a more solid-like structure than in samples without borax. Adding borax reduces tan δ values, particularly in samples with higher lignin content by enhancing the gel's solid-like properties through added cross-linking. Fig. 4G includes photos of the gel samples in both vertical and horizontal orientations. Hydrogels containing borax (right panel) maintain a clear shape and steady vertically without collapse, indicating a stronger network. In contrast, borax-free samples (left panel) show some deformation, especially in those with no or lower lignin content, confirming the structural reinforcement provided by borax.

Strain-sweep tests were also performed across a range of strains (from small amplitude oscillatory shear, i.e., SAOS, to large amplitude oscillatory shear, LAOS) to explain the strength of the dynamic bonds, their breaking, and re-forming in the gel samples. Fig. 4D and E present the storage and loss moduli of strain amplitude, focusing on the gel's response to increasing deformation. Neat CNC suspension shows type I strain-thinning behavior (both G' and G'' decreasing monotonically) Borax-free samples exhibit strain-softening behavior, decreasing G' as strain amplitude increases, particularly in lower lignin samples (5CNC-0 L-0B and 5CNC-0.5 L-0B). The 5CNC-1 L-0B sample, however, retains higher G' values at greater strain amplitudes, indicating stronger structural integrity under stress. The gradual decrease in G' with higher strain in samples with more lignin suggests that lignin enhances the gel's elasticity, enabling it to withstand greater strain without significant structural breakdown. Hydrogels with borax, G' remain stable even at higher strain levels before they begin to decrease, and this reduction is more gradual than in samples without borax. This pattern highlights the stabilizing effect of borax cross-linking, which strengthens the network and allows it to withstand strain better without compromising its structure. Among the borax-containing samples, 5CNC-1 L-2B shows the highest G' across the amplitude range due to aggregated lignin structures which reinforce the gels while deteriorating the network homogeneity as shown in SEM and POM images.

To summarize, the SEM, POM, and rheological analysis provide critical insights into the structural and mechanical properties of CNC-borax-lignin hydrogels which influences their flame retardancy. Lignin altered the porous structure of CNC-borax hydrogels, increasing the crosslinking density and enhancing the water-retention capacity, which can contribute to the flame-retardant mechanisms by providing both cooling effect and fuel dilution in a fire event. However, as the lignin content increased above Lignin/CNC = 0.5, the bond structure deteriorated, and pore homogeneity decreased, thus, water holding capacity was weakened due to agglomerations seen from SEM and POM analyses. Rheological analyses are also consistent with these findings. The frequency-independent high storage modulus (G') values indicate that the hydrogels exhibit a solid-like structure and can maintain their structural integrity under thermal stress. The CNC network was strengthened by dynamic boronate ester bonds, while lignin played a reinforcing effect (The sample stability and adhesion behavior were shown in Fig. S3 and S4). The sample stability and adhesion behavior were Thus, from the structure and rheology point of view, moderate lignin concentrations can be more effective in simultaneous actions of different fire prevention mechanisms, such as charring, thermal barrier, cooling, glassy layer formation, and fuel dilution.

3.3. Heat insulating behavior of composite hydrogels

The heat insulation behavior of the samples was assessed by heating the samples on a glass substrate placed on a hot plate that is held at a constant temperature 90 °C and monitoring the time evolution of the temperature at the top surface of the samples using an IR camera (see Fig. 5A for the sketch and Methods section for details). The thermal camera images captured at 10 min are also provided.

A blank substrate and pure water behavior, for which the temperature rises very rapidly, were also displayed. The profiles in the borax-free samples and the gel samples differ significantly (Fig. 5B). The samples without borax (5CNC-0 L-0B, 5CNC-0.5 L-0B, and 5CNC-1 L-0B) followed a trend similar to that of neat water, but with a delayed response, reaching approximately 90 °C within 10 min. Notably, the lignin-free CNC sample (5CNC-0 L-0B) exhibited a temperature rise delayed by about 2 min compared to the lignin-containing samples which display almost identical profiles. This can be due to the more hydrophilic nature of the CNCs which effectively slow down water loss compared to more hydrophobic lignin-containing samples. Although the decrease in water retention is partially attributed to the hydrophobic domains of lignin, it is important to note that this effect is not absolute. Other factors, such as lignin aggregation, reduced network uniformity, and possible disruption of hydrogen bonding within the CNC-borax matrix, may also contribute to the observed behavior.

The borax-containing gel samples, on the other hand, (5CNC-0 L-2B, 5CNC-0.5 L-2B, and 5CNC-1 L-2B) exhibited a much slower temperature increase compared to the borax-free samples, reaching the upper plateau in about 17 min. This provides strong evidence of the water-retention ability of the gel samples due to their highly porous network structure. While the addition of lignin in these samples also caused temperature rises earlier compared to the borax-free samples, however, in the gel samples, the highest lignin-containing gel (5CNC-1 L-2B) exhibited a more rapid increase. This is likely due to the disruption of the homogenous porous structure by the presence of lignin aggregates, allowing the bulk water to escape by evaporation.

To further support these observations, an isothermal drying test was performed to compare the water retention performance of the hydrogels (see Fig. S3). The results showed that water retention behavior varied with both lignin and borax content in the CNC hydrogels. To compare between the samples, water loss rates (dM/dt) were calculated from the slopes of the curves given in Fig. S5 in the first 15 min. The neat CNC hydrogel (5CNC-0 L-2B) showed a water loss rate of 0.24 g/min, which is significantly slower than the pure water (0.35 g/min), showing the effectiveness of the CNC network in holding water. As lignin was added, the water loss increased in the hydrogels, with rates of 0.27 g/min and 0.31 g/min for 5CNC-0.5 L-2B and 5CNC-1 L-2B samples, respectively. This trend is in line with the transient surface temperature profiles seen in the hot-plate experiment, verifying the interrelation between microstructure, physical interactions, and water release rates. Beyond the

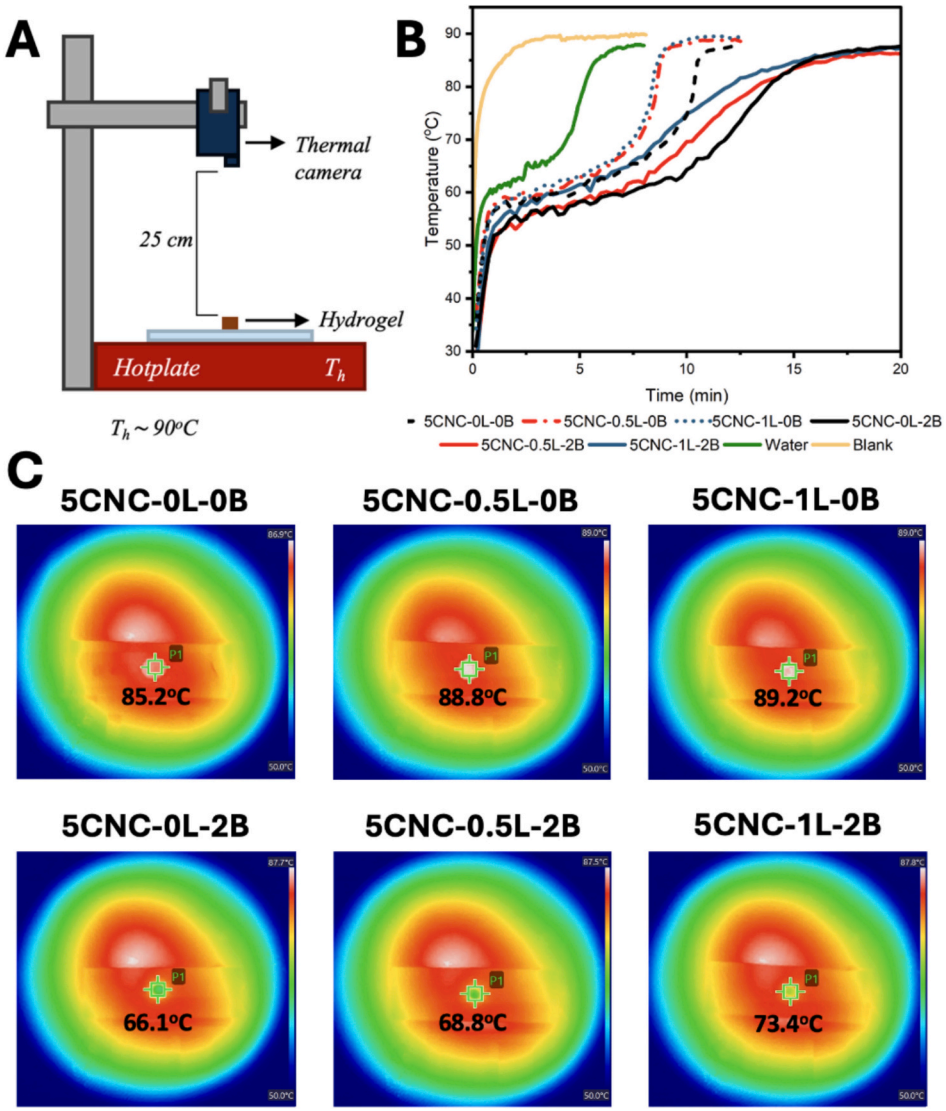


Fig. 5. (A) Schematic representation of the hot plate test setup. (B) Heating profiles of water and gel samples at the set temperature of 90 °C. (C) Thermal camera images of the samples at 10 min from hot plate test.

initial drying profiles in Fig. S5, it is interesting that the water loss rate of 5CNC-0.5 L-2B gel deviates significantly from its initial trendline during the later stages (after 30 min) of evaporation and finally retains a significant amount of water compared to the neat CNC and higher lignin-containing hydrogels. This behavior is attributed to a large fraction of bound water present in this sample exhibiting highly uniform and smaller pore structure (as shown in the SEMs), which provide a large surface area. The bound water can be released at higher temperatures, causing an additional flame-retardant functionality through cooling and fuel dilution mechanisms. Overall, these results showed that the lignin addition weakened the thermal barrier properties of the gel samples mainly due to the more rapid loss of water from the composites linked to the hydrophobic nature of the lignin and the disruption of the homogenous CNC network at elevated concentrations. Nonetheless, the CNC-borax hydrogel with a moderate lignin content (5CNC-0.5 L-2B) demonstrates superior water retention following the evaporation of bulk water, making it especially promising for sustained thermal shielding.

3.4. Thermogravimetric analysis of CNC-lignin-borax hydrogels

The thermal decomposition of CNC-based hydrogels with different lignin and borax levels was assessed using Thermogravimetric Analysis (TGA) and Derivative Thermogravimetric Analysis (DTG), as shown in 66. Fig. 6A provides the TGA and DTG curves for the individual components—CNC, lignin, and borax—as reference data. Two distinct pyrolysis stages are observed during the thermal decomposition of CNC. The first stage, marked by a DTG peak at 310.7 °C, corresponds to the decomposition of amorphous regions and sulfated groups, while the second stage, with a DTG peak at 379.6 °C, is attributed to the breakdown of non-sulfated cellulose segments [57,58]. Lignin decomposed over a broad temperature range, corresponding to the breakdown of its complex aromatic structure, with a prominent DTG peak at 382.1 °C. It exhibited relatively high thermal stability at higher temperatures. Borax undergoes a major mass loss at relatively low temperatures, with a DTG peak around 89.7 °C resulting from dehydration, losing 45.6 % of its initial mass up to 450 °C.

Figs. 6B through 6E present the thermal decomposition profiles for borax-free sol samples (Fig. 6B and C) and borax-containing gel samples (Fig. 6D and E) with varying lignin concentrations. The initial mass loss below 130 °C for all samples is due to the rapid evaporation of water upon heating. No significant differences are detected in the TGA/DTG curves upon adding lignin in the absence of borax during this stage (Fig. 6B and C). In these samples, the degradation stage occurs between 280 °C and 400 °C primarily corresponding to CNC breakdown. In the

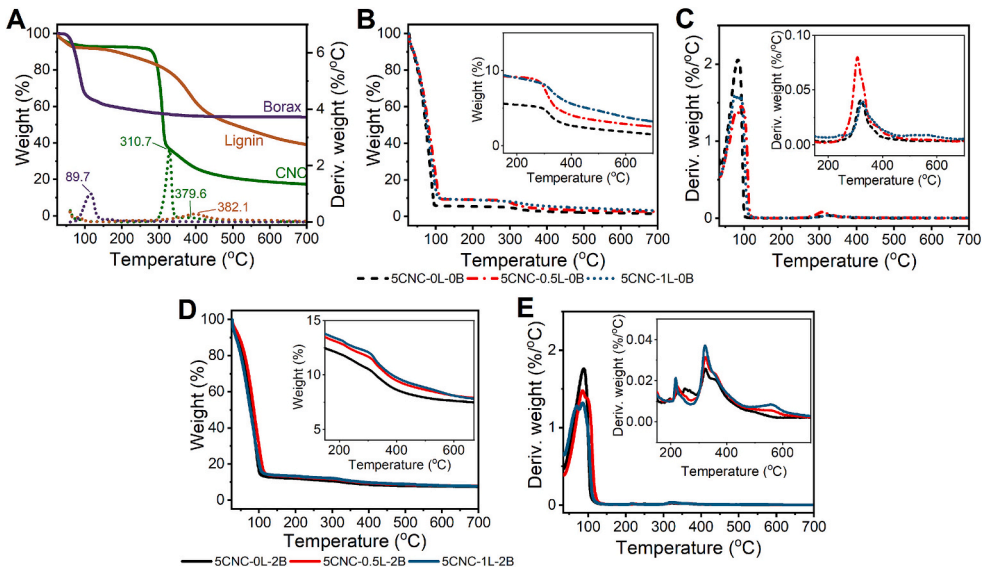


Fig. 6. (A) Weight loss and derivative weight curves of CNC, lignin, and borax. (B-E) Weight loss (TG) and derivative (DTG) curves of the gel samples: (B) TG graphs of 5CNC-0 L-0B, 5CNC-0.5 L-0B, and 5CNC-1 L-0B; (C) DTG graphs of 5CNC-0 L-0B, 5CNC-0.5 L-0B, and 5CNC-1 L-0B; (D) TG graphs of 5CNC-0 L-2B, 5CNC-0.5 L-2B, and 5CNC-1 L-2B; (E) DTG graphs of 5CNC-0 L-2B, 5CNC-0.5 L-2B, and 5CNC-1 L-2B.

5CNC-1 L-0B sample, the further decomposition above 400 °C, suggests a relatively slow breakdown of lignin. Increasing lignin content raises the char yield at higher temperatures; at 500 °C [59], corresponding to the end of lignin's main pyrolysis stage, the % residue for CNC-0 L-0B, 5CNC-0.5 L-0B, and 5CNC-1 L-0B samples were 2.2 %, 3.3 %, and 4.7 %, respectively (Table S3). The residue percentages for borax-free samples, ranging from 1 to 4 % at 700 °C, are lower than those of borax-containing gel samples (see Fig. 6D and E), which range from 7 to 8 % (Table S3). Borax addition reduces the peak mass loss rate during the first decomposition stage, associated with water evaporation, and this is consistent across all formulations. Between 300 °C and 400 °C, borax-containing hydrogels degrade more slowly, as indicated by the more gradual TGA slopes compared to borax-free counterparts. The DTG peaks (Fig. 6E) of borax-containing hydrogels within this temperature range shift to higher temperatures and exhibit lower values, especially in the 5CNC-1 L-2B sample, which has the highest lignin content. These findings were further substantiated by the analysis of the dried (water-free) samples (Table S3, Fig. S6). The lower decomposition rate and higher decomposition temperature observed upon borax incorporation suggest boron crosslinking, which hinders depolymerization [60]. A relatively smaller increase in mass loss rate which occurs at 200–300 °C in the borax-containing samples can be due to the dehydration of CNC catalyzed by dissolved boric acid which can enhance char formation [61]. The %residue at 500 °C for CNC-0 L-2B, 5CNC-0.5 L-2B, and 5CNC-1 L-2B samples were 7.9, 8.6 and 8.8 %, respectively (Table S3). Enhanced char formation upon borax incorporation was further confirmed by the analysis of dried films (Table S3). Thermal decomposition of dried CNC films (5CNC-0 L-0B) resulted in 8.6 % residue at 700 °C, while incorporating lignin (5CNC-1 L-0B) resulted in a char yield of 25.9 %. The addition of borax (5CNC-1 L-2B) further increased the char yield to 70.5 %. This effect is attributed to boric acid–catalyzed dehydration which promotes charring.

3.5. Response of the composite hydrogels to fire

The high water retention capacity of hydrogels plays a crucial role in their flame-retardant activity, particularly in delaying ignition. When applied to wooden substrates, hydrogels significantly reduce flammability, making ignition difficult in any orientation. Moreover, their tendency to dehydrate before or during testing—especially under high external heat fluxes, such as 50 kW/m^2 used in cone calorimeter—poses a challenge in assessing their fire-retardant performance over time. In this study, we investigated the burn-through resistance and ease of extinction of hydrogel-coated wood samples, along with their charring ability using simple yet effective techniques tailored to evaluate the efficacy of hydrogels.

The increase in char formation and residue amount with lignin and borax content was macroscopically observed in the spoon test images. Fig. 7A shows that the lignin-free sample (5CNC-0 L-0B) left no visible char residue after testing. In contrast, in the 5CNC-0.5 L-0B sample, some char formation was observed, but its quantity remained quite low. While lignin influences char formation, the lack of borax crosslinker in these samples results in an uncontrolled burning process. However, as shown in Fig. 7B, the amount of char residue increased significantly with the addition of borax, even in the absence of lignin. The residual char volume increased monotonically and significantly with the lignin content as seen for 5CNC-0.5 L-2B and 5CNC-1 L-2B samples. These suggest the synergistic effects of borax and lignin in the formation of a stable char layer. Lignin has a highly aromatic structure which contributes to the formation of thermally stable carbon-rich residues and increases the rate of carbonization [19,62,63].

On the other hand, borax facilitates the formation of more ordered carbon structures by strengthening the hydrogen bonding within the CNC-lignin-borax system [58,64,65]. Upon heating borax first releases water, converting it to sodium borate, which melts at around 735 °C and forms a glassy layer [66,67]. Similarly boric acid yields boric oxide which also forms a low-melting temperature glass [68]. This glassy layer can cover the char, limiting oxygen diffusion and reducing oxidation of the underlying char [46,60].

The experimental set-up designed to assess the ease of extinction is shown in Fig. 8A (see also the Methods section). Fig. 8B illustrates the effect of hydrogel composition on the flame-retardant properties of wooden sticks, where a 0.25 cm portion along the length of the stick was coated with 12.5 mg of gel. In the 5CNC-0 L-2B and 5CNC-1 L-2B samples, flames passed through the gel-coated area, indicating that these formulations were insufficient to stop flame propagation over the applied length. However, in the 5CNC-0.5 L-2B sample, the flame was almost immediately extinguished upon reaching the coated region, indicating that the gel effectively prevented the flame progression. For all gel samples (5CNC-0 L-2B, 5CNC-0.5 L-2B and 5CNC-1 L-2B), the flame was extinguished when it reached a 0.5 cm hydrogel-coated portion (Fig. S7). The results indicate that coating a 0.5 cm portion of

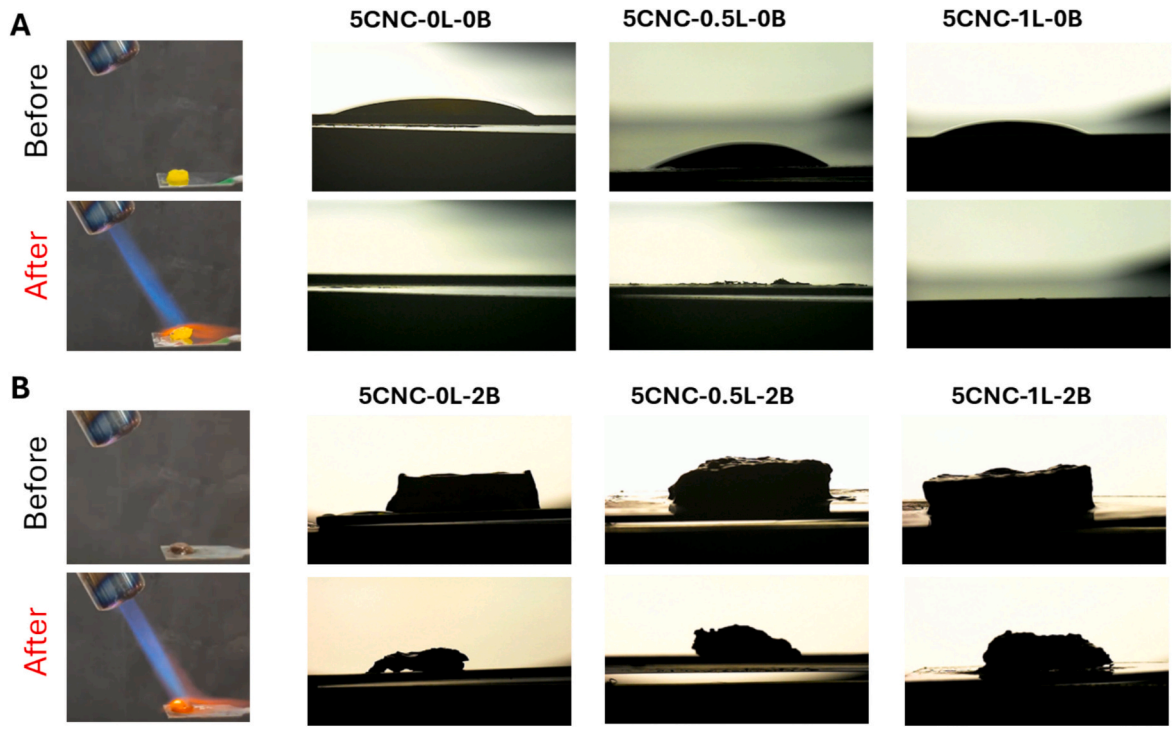


Fig. 7. Gel sample images before and as exposed to flame. The cross-section images before and after the test for (A) 5CNC-0 L-0B, 5CNC-0.5 L-0B, and 5CNC-1 L-0B; (B) 5CNC-0 L-2B, 5CNC-0.5 L-2B, and 5CNC-1 L-2B.

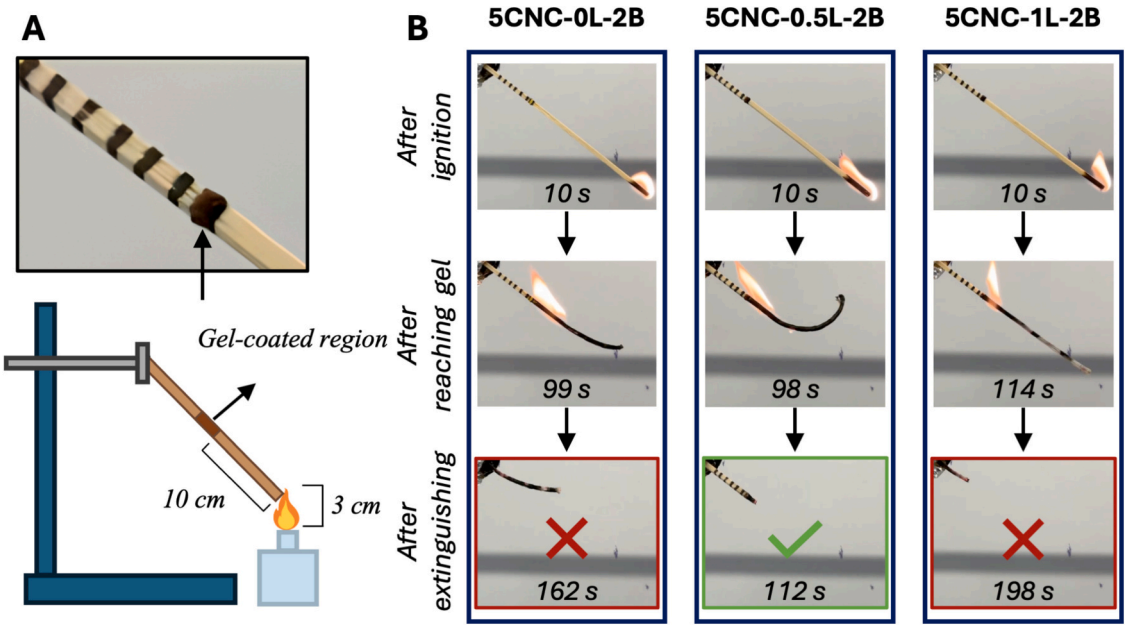


Fig. 8. (A) Schematic representation of 45-degree flammability test setup. (B) 45-degree flammability of 2.5 mm gel-coated wood sticks after flame impingement, reaching the gel coated portion and after extinguishing. See 5 mm gel-coated wood stick images in Fig. S7 in SI.

the stick with 25 mg of hydrogel effectively served as a barrier, preventing the flame from spreading beyond the coated area. According to POM analyses (Fig. 3C), increasing lignin content leads to agglomeration within the hydrogel matrix and may disrupt the gel structure. This disruption prevents the formation of homogeneous carbon structure and hinders the stability of char. Although lignin enhances flame retardancy by promoting carbonization, excessive lignin content can lead to agglomeration, disrupting the carbonization process and reducing flame-retardant performance. Therefore, achieving a balanced ratio of lignin and borax content is crucial for maintaining gel uniformity, enabling effective flame suppression, and ensuring thermal stability.

Fig. 9 presents the burn-through resistance of wooden blocks coated with the hydrogels upon exposure to a blowtorch (see also Methods section for details). The uncoated dry substrate shows heavy charring and cracking, indicating significant damage from direct flame exposure. The flames reached the rear surface of the wooden substrate in approximately 7 min. The borax-containing hydrogel (5CNC-0 L-2B) formed a protective char layer that adhered well to the surface reducing

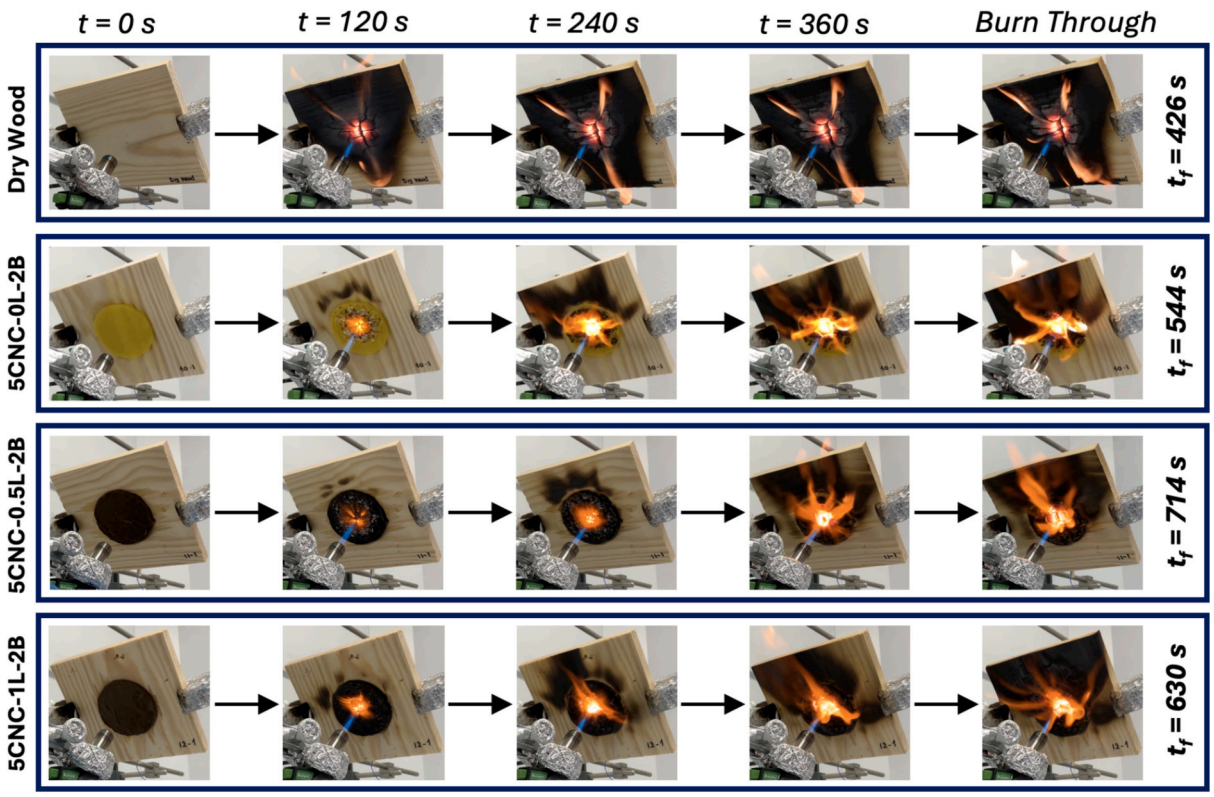


Fig. 9. Burn-through progress of dry and coated with 5CNC-0 L-2B, 5CNC-0.5 L-2B and 5CNC-1 L-2B hydrogels wood panels.

flame penetration and protecting the substrate, yielding the burn through time of 9 min. In 5CNC-0 L-2B, the absence of lignin, a strong charring agent, resulted in limited charring and severe cracking in the wooden block as seen in the residue images from the burn-through tests (Fig. S8). The incorporation of lignin (5CNC-0.5 L-2B) strengthens the char, forming a dense, uniform layer that acts as a barrier and minimizes substrate damage. The 5CNC-0.5 L-2B hydrogel demonstrated the highest performance, with a burn-through time of 12 min—representing an increase of approximately 71 % and 33 % compared to uncoated and neat CNC-coated wood, respectively. This performance can be partly attributed to its relatively higher water content, which evaporates endothermically during burning, cooling down the substrate and diluting the combustible gases. While the higher lignin content in 5CNC-1 L-2B, also contributed to the formation of a robust char layer, but the burn-through time (≈10 min) is much shorter than 5CNC-0.5 L-2B, and slightly above the results from the lignin-free CNC hydrogel coating. According to microstructure analyses in Fig. 3C, this reduction in performance can be attributed to lignin agglomeration, which disrupts char integrity. In addition, the agglomerated lignin results in heterogeneities in the network of CNC, causing water to escape relatively easily (see also Fig.5 and Fig.S5) compared to 5CNC-0.5 L-2B and leading to inefficient cooling.

The flame propagation and fire prevention performance of the hydrogels were evaluated using a vertical flammability test setup. Wooden sticks were exposed to flame for 10 s to examine the vertical flame propagation in Fig. 10. The 2-g hydrogel-coated sticks successfully self-extinguished the flames (Fig. S9). Among the tested samples, 5CNC-0.5 L-2B exhibited the shortest after flame duration of 46 s, while the lignin-free sample (5CNC-0 L-2B) burned for 71 s. These results once again confirmed the effect of lignin on self-extinguishing behavior. To simulate more demanding conditions, the hydrogel coating weight was reduced to 1 g per surface in the subsequent experiments. Out of the six wooden sticks coated with 5CNC-0 L-2B hydrogel, only three specimens exhibited self-extinguishing behavior whereas the rest burned completely. These results indicate that the flame-retardant performance of the formulation containing only borax formulations may be inconsistent. In contrast, all six specimens coated with 5CNC-0.5 L-2B exhibited self-extinguishing behavior. This improvement may be due to the cooling and fuel dilution effects exhibited by the water molecules trapped in the shrinking pores in the presence of lignin. Furthermore, lignin formed a dense, protective char layer that minimized substrate damage, leading to smaller cracks in the underlying wood (Fig. S10). The 5CNC-1 L-2B hydrogel effectively extinguished the flames in four out of the six wooden specimens but burning progressed in the other two, suggesting that while the addition of lignin contributes to flame retardancy, excessive lignin content can compromise the hydrogel's structure and reduce its water retention capacity, thus affecting its overall flame-retardant performance. When we compare the lignin-containing hydrogels in the tests where the flame was completely extinguished, it was observed that 5CNC-0.5 L-2B provided extinguishing in a shorter time such as 50 s.

The efficacy of the glassy char barrier formed during burning was assessed by igniting the 2-g gel-coated wooden specimens after drying them at 60 °C for 1 h, a duration sufficient for the complete removal of water from the freshly prepared gels (Fig. 10 right panel and see Fig. S11 for post-test results). While the wet-state tests emphasize the effect of water molecules in cooling and oxygen dilution, the dry-state tests more clearly reveal the direct effects of material structure and chemical constituents on thermal stability and flame-extinguishing ability. This test is particularly critical for understanding the role of lignin such as promoting charring and forming a glass-like protective layer. The glassy barrier char layer formed after the test by the 5CNC-0.5 L-2B and 5CNC-1 L-2B hydrogels effectively served as a protective barrier and limited the flame progression.

This study introduces a novel flame-retardant hydrogel system based on cellulose nanocrystals, borax, and lignin—each selected for bio renewability and functional contribution. The combined properties of these components result in a hydrogel that not only improves fire safety

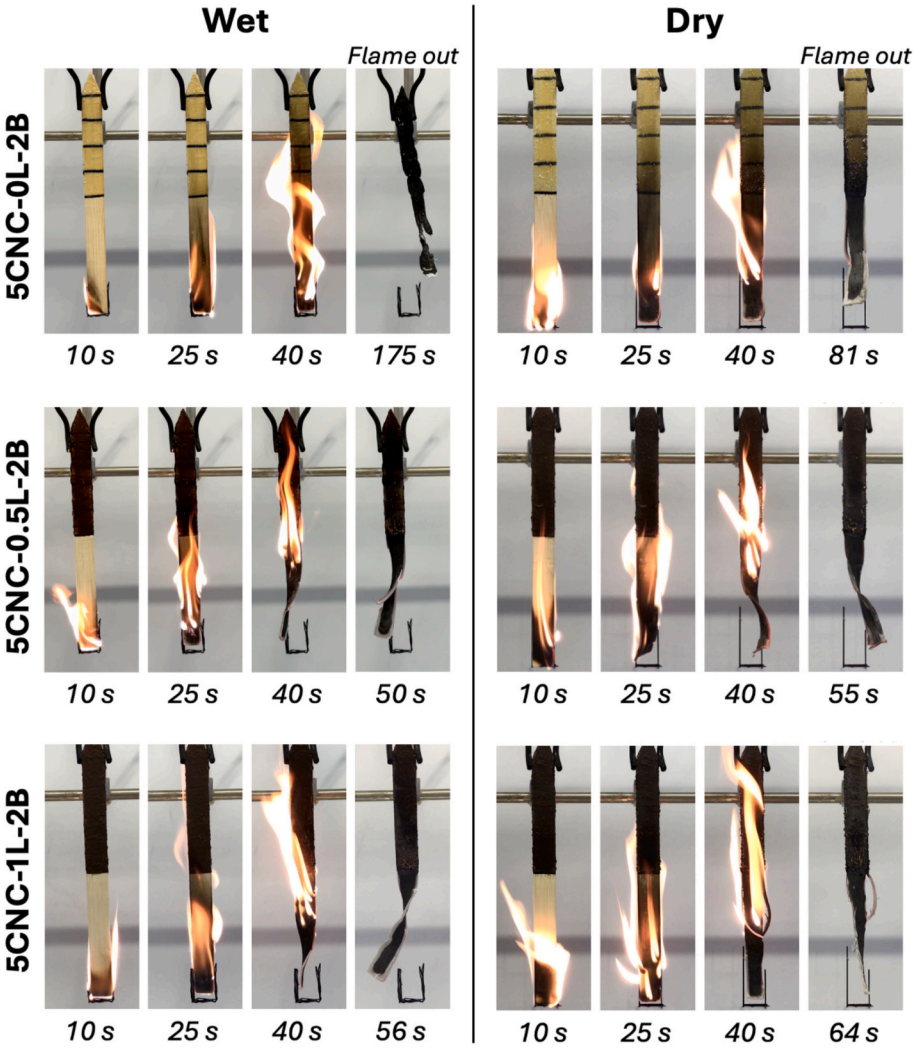


Fig. 10. Vertical flammability test on wooden bar samples coated with 5CNC-0 L-2B, 5CNC-0.5 L-2B, and 5CNC-1 L-2B hydrogels. In the wet state, each side of the specimen was coated with 1-g of gel. In the dry state, each side of the specimens was coated with 2-g of gel.

but also retains mechanical stability and structural integrity under thermal stress. The developed hydrogel system can effectively overcome a known limitation associated with conventional hydrogel-based fire retardants and maintain its fire-retardant function after dehydration. The results in vertical combustion tests and the consistent formation of a char layer on the wood surface demonstrate the practicality of this system as a surface coating for fire protection purposes. Beyond its immediate performance, the study also provides important insights into the fire-retardant behavior of the components together within hydrogel networks and suggests a new approach to the development of fire-resistant materials that can be used in areas such as construction, forestry and textiles.

4. Conclusion

In this study, CNC-borax hydrogels enriched with lignin were developed and the flame-retardant performance of these hydrogels was systematically investigated in terms of their structural, rheological, thermal, and flammability properties. At moderate concentrations, lignin increased the formation of hydrogen bonds, resulting in a more dense and homogeneous structure in the hydrogel matrix, which led to the shrinkage of pores. The reduced pore size increased the water retention capacity of the hydrogel during combustion. The water molecules retained in the gel contributed to the flame-retardant performance through cooling and fuel dilution mechanisms. The incorporation of lignin into the CNC-borax system led to the formation of a dense glassy char layer which serves as an effective barrier against heat and oxygen diffusion. Higher lignin content in composite hydrogels resulted in agglomeration, disrupting the homogeneity and binding order within the hydrogel matrix. This disruption reduced the pore size and decreased the water retention and overall flame-retardant performance. This study highlights the potential of CNC-borax-lignin hydrogels as environmentally friendly coatings with superior flame-retardant properties. The findings provide valuable insights into the design of lignin-based flame-retardant materials and enable the development of sustainable and effective solutions to combat forest and wood fires.

CRediT authorship contribution statement

Aybüke Özkan: Writing – original draft, Visualization, Investigation, Formal analysis, Data curation. **Ezgi Mıhlayanlar:** Visualization, Formal analysis, Data curation. **Emine Ayşe Turhan:** Writing – review & editing, Visualization, Formal analysis, Data curation. **Ebru Sarıoğlu:** Writing – review & editing, Formal analysis, Data curation. **Paul Berlu:** Visualization, Formal analysis, Data curation. **Elif Kaynak:** Writing – review & editing, Validation, Methodology, Investigation, Formal analysis, Data curation. **Erkan Senses:** Writing – review & editing, Visualization, Validation, Supervision, Resources, Project

administration, Methodology, Investigation, Funding acquisition, Conceptualization.

Declaration of competing interest

The authors declare that they have no known competing financial interests or personal relationships that could have appeared to influence the work reported in this paper.

Acknowledgement

This work is supported by 1001 Program of The Scientific and Technological Research Council of Turkey (TÜBİTAK) (Grant no: 222Z106). We thank Dr. Barış Yağci of Koc University Surface Science and Technology Center (KUYTAM) for his help with SEM images and XPS measurements. We thank Prof. Alper Uzun, Ms. Nitasha Habib and Ms. Zeynep Demir for their help with the thermogravimetric measurements.

Appendix A. Supplementary data

Supplementary data to this article can be found online at https://doi.org/10.1016/j.ijbiomac.2025.144007.

References

[1] D.L. Martell, A review of recent forest and wildland fire management decision support systems research, Curr. For. Rep. 1 (2015) 128–137.
[2] J. Hai, L. Zhang, C. Gao, H. Wang, J. Wu, How does fire suppression alter the wildfire regime? A systematic review. *Fire* 6 (11) (2023) 424.
[3] L. Hu, H. Zhu, L. Xie, B. Li, B. Qu, Q. Liao, R. Tao, Fire prevention and extinguishing technologies in coal spontaneous combustion: a bibliometric and systematic review, J. Therm. Anal. Calorim. (2024) 1–25.
[4] Z. Yu, Y. Wan, Y. Qin, J.-P. Guan, X.-W. Cheng, X. Wang, S. Ouyang, X. Qu, Z. Zhu, J. Wang, High fire safety thermal protective composite aerogel with efficient thermal insulation and reversible fire warning performance for firefighting clothing, Chem. Eng. J. 477 (2023) 147187.
[5] X.F. Cui, W.J. Zheng, W. Zou, X.Y. Liu, H. Yang, J. Yan, Y. Gao, Water-retaining, tough and self-healing hydrogels and their uses as fire-resistant materials, Polym. Chem. 10 (37) (2019) 5151–5158.
[6] X. Qian, N. Mu, X. Zhao, C. Shi, S. Jiang, M. Wan, B. Yu, Novel self-healing and recyclable fire-retardant polyvinyl alcohol/borax hydrogel coatings for the fire safety of rigid polyurethane foam, Soft Matter 19 (32) (2023) 6097–6107.
[7] J. Mastalska-Popławska, Ł. Wójcik, P. Izak, Applications of hydrogels with fire retardant properties—a review, J. Sol-Gel Sci. Technol. 105 (3) (2023) 608–624.
[8] H. Vahabi, F. Gholami, M. Tomas, E. Movahedifar, M.K. Yazdi, M.R. Saeb, Hydrogel and aerogel-based flame-retardant polymeric materials: a review, J. Vinyl Addit. Technol. 30 (1) (2024) 5–25.
[9] G. Grant, J. Brenton, D. Drysdale, Fire suppression by water sprays, Prog. Energy Combust. Sci. 26 (2) (2000) 79–130.
[10] J. Mawhinney, B. Dlugogorski, A. Kim, A closer look at the fire extinguishing properties of water mist, Fire Safety Sci. 4 (1) (1994) 47–60.
[11] Z. Dai, C. Huang, Y. Chen, M. Zhong, W. He, Experimental study on fire extinguishing efficiency of polymer hydrogel fire extinguishing agent in pine-fir mixed coniferous forest fires, Case Stud. Thermal Eng. 64 (2024) 105413.
[12] G. Li, Q. Wang, G. Liu, M. Yao, Y. Wang, Y. Li, K. Lin, X. Liu, Hydrogel Extinguishants, Nanomaterials 14 (13) (2024) 1128.
[13] Z. Yu, J. Liu, A. Suryawanshi, H. He, Y. Wang, Y. Zhao, Thermal insulating and fire-retarding behavior of treated cotton fabrics with a novel high water-retaining hydrogel used in thermal protective clothing, Cellulose 28 (2021) 2581–2597.
[14] S. Bashir, M. Hina, J. Iqbal, A. Rajpar, M. Mujtaba, N. Alghamdi, S. Wageh, K. Ramesh, S. Ramesh, Fundamental concepts of hydrogels: synthesis, properties, and their applications, Polymers 12 (11) (2020) 2702.
[15] S. Thakur, B. Sharma, A. Verma, J. Chaudhary, S. Tamulevicius, V.K. Thakur, Recent progress in sodium alginate based sustainable hydrogels for environmental applications, J. Clean. Prod. 198 (2018) 143–159.
[16] H. Nabipour, H. Shi, X. Wang, X. Hu, L. Song, Y. Hu, Flame retardant cellulose-based hybrid hydrogels for firefighting and fire prevention, Fire. Technol 58 (4) (2022) 2077–2091.
[17] G. Xiao, F. Li, Y. Li, C. Chen, C. Chen, Q. Liu, W. Chen, A novel biomass material composite hydrogel based on sodium alginate, Colloids Surf. A Physicochem. Eng. Asp. 648 (2022) 129383.
[18] N. Mandlekar, A. Cayla, F. Rault, S. Giraud, F. Salaün, G. Malucelli, J.-P. Guan, An overview on the use of lignin and its derivatives in fire retardant polymer systems, Lignin-trends and applications 9 (2018) 207–231.
[19] H. Yang, B. Yu, X. Xu, S. Bourbigot, H. Wang, P. Song, Lignin-derived bio-based flame retardants toward high-performance sustainable polymeric materials, Green Chem. 22 (7) (2020) 2129–2161.
[20] X. Zhang, J. Yang, L. Weng, W. Fan, Y. Xu, Enhanced mechanical performance of cellulose nanocrystal doped eco-friendly calcium-alginate based bio-composite fiber with superior flame retardancy, Text. Res. J. 92 (11–12) (2022) 1820–1829.
[21] S. Won, M. Jung, J. Bang, S.Y. Cho, I.-G. Choi, H.W. Kwak, Lignin-based flame retardant via sequential purification-nanoparticle formation, and NP coupled chemical modification, Int. J. Biol. Macromol. 281 (2024) 136499.
[22] Q. Wu, F. Ran, L. Dai, C. Li, R. Li, C. Si, A functional lignin-based nanofiller for flame-retardant blend, Int. J. Biol. Macromol. 190 (2021) 390–395.
[23] N.N. Solihat, A.F. Hidayat, M.N.A.M. Taib, M.H. Hussin, S.H. Lee, M.A.A. Ghani, S. S.O.A. Edrus, H. Vahabi, W. Fatriasari, Recent developments in flame-retardant lignin-based biocomposite: manufacturing, and characterization, J. Polym. Environ. 30 (11) (2022) 4517–4537.
[24] Y. Yang, L. Zhang, J. Zhang, Y. Ren, H. Huo, X. Zhang, K. Huang, M. Rezakazemi, Z. Zhang, Fabrication of environmentally, high-strength, fire-retardant biocomposites from small-diameter wood lignin in situ reinforced cellulose matrix, Adv. Compos. Hybrid Mater. 6 (4) (2023) 140.
[25] S.C. Agwuncha, C. Anusionwu, E. Sadiku, Eco-friendly lignin-based flame retardant from different polymeric materials, in: Biomaterials as Green Flame Retardants, Springer, 2024, pp. 231–258.
[26] Q. Cen, S. Chen, D. Yang, D. Zheng, X. Qiu, Full bio-based aerogel incorporating lignin for excellent flame retardancy, mechanical resistance, and thermal insulation, ACS Sustain. Chem. Eng. 11 (11) (2023) 4473–4484.
[27] C. Li, B. Wang, L. Zhou, X. Hou, S. Su, Effects of lignin-based flame retardants on flame-retardancy and insulation performances of epoxy resin composites, Iran. Polym. J. 31 (8) (2022) 949–962.
[28] K. Liu, H. Du, T. Zheng, W. Liu, M. Zhang, H. Liu, X. Zhang, C. Si, Lignin-containing cellulose nanomaterials: preparation and applications, Green Chem. 23 (24) (2021) 9723–9746.
[29] D. Rico-García, L. Ruiz-Rubio, L. Pérez-Alvarez, S.L. Hernández-Olmos, G. L. Guerrero-Ramírez, J.L. Vilas-Vilela, Lignin-based hydrogels: Synthesis and applications, Polymers 12 (1) (2020) 81.
[30] F. Laoutid, H. Vahabi, M.R. Saeb, P. Dubois, Lignin as a flame retardant for biopolymers, in: Micro and Nanolignin in Aqueous Dispersions and Polymers, Elsevier, 2022, pp. 173–202.
[31] A.A. Moud, M. Kamkar, A. Sanati-Nezhad, S.H. Hejazi, Suspensions and hydrogels of cellulose nanocrystals (CNCs): characterization using microscopy and rheology, Cellulose 29 (7) (2022) 3621–3653.
[32] D. Łukawski, W. Grześkowiak, A. Lekawa-Raus, M. Widelicka, F. Lisiecki, A. Dudkowiak, Flame retardant effect of lignin/carbon nanotubes/potassium carbonate composite coatings on cotton roving, Cellulose 27 (2020) 7271–7281.
[33] L. Liu, B. Shi, A. Zhang, Y. Xue, J. Zhang, J. Dai, M. Hassanpour, L.-C. Tang, Y. Shi, P. Song, A polyphosphoramide-grafted lignin enabled thermostable and fire-retardant polylactide with preserved mechanical properties, Compos. A: Appl. Sci. Manuf. 160 (2022) 107028.
[34] A. Cayla, F. Rault, S. Giraud, F. Salaün, V. Fierro, A. Celzard, PLA with intumescent system containing lignin and ammonium polyphosphate for flame retardant textile, Polymers 8 (9) (2016) 331.
[35] N. Mandlekar, A. Cayla, F. Rault, S. Giraud, F. Salaün, J. Guan, Valorization of industrial lignin as biobased carbon source in fire retardant system for polyamide 11 blends, Polymers 11 (1) (2019) 180.
[36] N. Mandlekar, A. Cayla, F. Rault, S. Giraud, F. Salaün, G. Malucelli, J. Guan, Intumescent formulations based on lignin and phosphinates for the bio-based textiles, in: IOP Conference Series, Materials Science and Engineering, 2017.
[37] N. Koparipek-Arslan, E. Kaynak-Uraz, E. Senses, Dynamically bonded cellulose nanocrystal hydrogels: structure, rheology and fire prevention performance, Carbohydr. Polym. 334 (2024) 122013.
[38] Y. Meng, J. Lu, Y. Cheng, Q. Li, H. Wang, Lignin-based hydrogels: a review of preparation, properties, and application, Int. J. Biol. Macromol. 135 (2019) 1006–1019.
[39] A.L. Mohamed, A.G. Hassabo, Flame retardant of cellulosic materials and their composites, Flame retardants: polymer blends, composites and nanocomposites (2015) 247–314.
[40] K.A. Salmeia, M. Jovic, A. Ragaisiene, Z. Rukuiziene, R. Milasius, D. Mikucioniene, S. Gaan, Flammability of cellulose-based fibers and the effect of structure of phosphorus compounds on their flame retardancy, Polymers 8 (8) (2016) 293.
[41] B.W. Chieng, S.H. Lee, N.A. Ibrahim, Y.Y. Then, Y.Y. Loo, Isolation and characterization of cellulose nanocrystals from oil palm mesocarp fiber, Polymers 9 (8) (2017) 355.
[42] J. Han, Y. Yue, Q. Wu, C. Huang, H. Pan, X. Zhan, C. Mei, X. Xu, Effects of nanocellulose on the structure and properties of poly (vinyl alcohol)-borax hybrid foams, Cellulose 24 (2017) 4433–4448.
[43] B. Lu, F. Lin, X. Jiang, J. Cheng, Q. Lu, J. Song, C. Chen, B. Huang, One-pot assembly of microfibrillated cellulose reinforced PVA–borax hydrogels with self-healing and pH-responsive properties, ACS Sustain. Chem. Eng. 5 (1) (2017) 948–956.
[44] S. Spoljaric, A. Salminen, N.D. Luong, J. Seppälä, Stable, self-healing hydrogels from nanofibrillated cellulose, poly (vinyl alcohol) and borax via reversible crosslinking, Eur. Polym. J. 56 (2014) 105–117.
[45] Y. Tang, K. Petropoulos, F. Kurth, H. Gao, D. Migliorelli, O. Guenat, S. Generelli, Screen-printed glucose sensors modified with cellulose nanocrystals (CNCs) for cell culture monitoring, Biosensors 10 (9) (2020) 125.
[46] S. Tanpichai, F. Phoothong, A. Boonmahitthisud, Superabsorbent cellulose-based hydrogels cross-liked with borax, Sci. Rep. 12 (1) (2022) 8920.
[47] R. Díaz de León, E. Guzmán, R. López González, A. Díaz Elizondo, I. Magaña, G. Neira, A. Castañeda Facio, L. Valencia, Surface modification of cellulose

nanocrystals with lactone monomers via plasma-induced polymerization and their application in ABS nanocomposites, Polymers 13 (16) (2021) 2699.
[48] E.L. de Paula, F. Roig, A. Mas, J.-P. Habas, V. Mano, F.V. Pereira, J.-J. Robin, Effect of surface-grafted cellulose nanocrystals on the thermal and mechanical properties of PLLA based nanocomposites, Eur. Polym. J. 84 (2016) 173–187.
[49] H. Wang, S. Fang, M. Zuo, Z. Li, X. Yu, X. Tang, Y. Sun, S. Yang, X. Zeng, L. Lin, Removal of copper ions by cellulose nanocrystal-based hydrogel and reduced adsorbents for its catalytic properties, Cellulose 29 (8) (2022) 4525–4537.
[50] D. Chen, K. Cen, X. Zhuang, Z. Gan, J. Zhou, Y. Zhang, H. Zhang, Insight into biomass pyrolysis mechanism based on cellulose, hemicellulose, and lignin: Evolution of volatiles and kinetics, elucidation of reaction pathways, and characterization of gas, biochar and bio-oil, Combust. Flame 242 (2022) 112142.
[51] H. Shen, X. Zheng, L. Dong, D. Huang, Bioinspired high-strength borate cross-linked microfibrillated cellulose composite laminate with self-extinguishing flame Retardance and Superhydrophobicity for self-cleaning, ACS Omega 8 (44) (2023) 41458–41468.
[52] C. Lane, D. Rode, T. Rösgen, Birefringent properties of aqueous cellulose nanocrystal suspensions, Cellulose 29 (11) (2022) 6093–6107.
[53] R. Kádár, S. Spirk, T. Nypelo, Cellulose nanocrystal liquid crystal phases: Progress and challenges in characterization using rheology coupled to optics, scattering, and spectroscopy, ACS Nano 15 (5) (2021) 7931–7945.
[54] E. Kushan, E. Senses, Thermoresponsive and injectable composite hydrogels of cellulose nanocrystals and pluronic F127, ACS Appl. Bio Mater. 4 (4) (2021) 3507–3517.
[55] S. Shafiei-Sabet, W.Y. Hamad, S.G. Hatzikiriakos, Rheology of nanocrystalline cellulose aqueous suspensions, Langmuir 28 (49) (2012) 17124–17133.
[56] S. Sugiarto, R.R. Pong, Y.C. Tan, Y. Leow, T. Sathasivam, Q. Zhu, X.J. Lou, D. Kai, Advances in sustainable polymeric materials from lignocellulosic biomass, Mater. Today Chem. 26 (2022) 101022.
[57] A. Merlini, C. Claumann, A.W. Zibetti, A. Coirolo, T. Rieg, R.A. Machado, Kinetic study of the thermal decomposition of cellulose nanocrystals with different crystal structures and morphologies, Ind. Eng. Chem. Res. 59 (30) (2020) 13428–13439.
[58] N. Wang, E. Ding, R. Cheng, Thermal degradation behaviors of spherical cellulose nanocrystals with sulfate groups, Polymer 48 (12) (2007) 3486–3493.
[59] Q. Zheng, D. Zhang, P. Fu, A. Wang, Y. Sun, Z. Li, Q. Fan, Insight into the fast pyrolysis of lignin: unraveling the role of volatile evolving and char structural evolution, Chem. Eng. J. 437 (2022) 135316.
[60] B. Wicklein, D. Kocjan, F. Carosio, G. Camino, L. Bergström, Tuning the nanocellulose–borate interaction to achieve highly flame retardant hybrid materials, Chem. Mater. 28 (7) (2016) 1985–1989.
[61] F. D'Acierno, W.Y. Hamad, C.A. Michal, M.J. MacLachlan, Thermal degradation of cellulose filaments and nanocrystals, Biomacromolecules 21 (8) (2020) 3374–3386.
[62] J. Li, B. Li, X. Zhang, R. Su, The study of flame retardants on thermal degradation and charring process of manchurian ash lignin in the condensed phase, Polym. Degrad. Stab. 72 (3) (2001) 493–498.
[63] Y. Sekiguchi, J.S. Frye, F. Shafizadeh, Structure and formation of cellulosic chars, J. Appl. Polym. Sci. 28 (11) (1983) 3513–3525.
[64] M.W. Smith, B. Pecha, G. Helms, L. Scudiero, M. Garcia-Perez, Chemical and morphological evaluation of chars produced from primary biomass constituents: cellulose, xylan, and lignin, Biomass Bioenergy 104 (2017) 17–35.
[65] I. Turku, A. Rohumaa, T. Tirri, L. Pulkkinen, Progress in achieving fire-retarding cellulose-derived Nano/micromaterial-based thin films/coatings and aerogels: a review, Fire 7 (1) (2024) 31.
[66] J. Faghihi, J. Morshedian, S. Ahmadi, Effect of alumina trihydrate and borax on fire retardancy and mechanical properties of high density polyethylene (HDPE) compounds, Polym. Polym. Compos. 18 (2) (2010) 113–122.
[67] I. Waclawska, Thermal decomposition of borax, J. Therm. Anal. 43 (1995) 261–269.
[68] K.K. Shen, R. O'Connor, Flame Retardants: Borates, An AZ reference, Plastics additives, 1998, pp. 268–276.